Relation between structure, stress, and magnetism in Co/W(001)

W. Wulfhekel, T. Gutjahr-Löser, F. Zavaliche, D. Sander, and J. Kirschner
Max-Planck-Institut für Mikrostrukturphysik, Weinberg 2, 06120 Halle, Germany
(Received 19 March 2001; published 21 September 2001)

We present a study of the structure of Co/W(001) determined by low-energy electron diffraction, the film stress measured by a bending thin substrate, and the film morphology measured by scanning tunneling microscopy in combination with *in situ* magnetic characterization by the magneto-optic Kerr effect. Different regimes in the stress behavior during growth are correlated to surface effects and structural and morphological changes in the Co film. Initially a compressive stress is observed as the result of the lower surface free energy of Co compared to W, followed by a tensile stress due to the large misfit between film and substrate. The structural transition from bcc to hcp Co as well as dislocation formation is clearly observed in the stress measurements and by low-energy electron diffraction and scanning tunneling microscopy. Additionally, the morphology of the films is correlated with the magnetic properties and a new surface alloy at submonolayer coverages is reported.

DOI: 10.1103/PhysRevB.64.144422 PACS number(s): 75.70.Ak, 75.30.Gw, 61.72.Ff, 75.80.+q

I. INTRODUCTION

Stress, strain, morphology, and the magnetic behavior of magnetic ultrathin heteroepitaxial films are intimately linked properties.[1–3] By choosing an appropriate substrate, the film structure can be selected, e.g., bcc, fcc, or hcp Co on GaAs(001), Cu(001), and Au(111), respectively.[4–8] Additionally, the misfit between the magnetic film and the substrate induces strain and stress in the magnetic films that influence the growth mode.[9] The structure and the morphology as well as the strain determine the magnetic properties of the films.[1–3] Also the exchange interaction and by this the Curie temperature have been proposed to depend on the structure and the morphology.[7,10] Magnetic anisotropy is influenced directly by the structure and the morphology[11–13] and indirectly by the strain via the magnetoelastic coupling.[14–18] Hence, a detailed understanding of all underlying principles is essential to tailor the magnetic properties of ultrathin films. In this study, we intend to illuminate the role of the film stress and strain on structure, morphology, and magnetism of Co films on W(001).

There have been only a few studies dealing with Co on W(001), so far. Wormeester *et al.* concluded from reflection high-energy electron diffraction (RHEED) patterns that Co grows pseudomorphically in the bcc structure on W(001) up to a coverage of $\approx$2.4 monolayers (ML).[19,20] At higher coverages, the layer cannot withstand the high biaxial strain of 9% and the bcc structure becomes unstable and transforms into a rough hcp Co film consisting of islands with the epitaxial relation $(11\bar{2}0)_{\mathrm{Co}}$ parallel to $(001)_{\mathrm{W}}$.

II. EXPERIMENT

Our experiments were carried out in two separate ultrahigh-vacuum (UHV) chambers at base pressures below 7×10^{-11} mbar. Both setups are equipped with Auger electron spectroscopy (AES) and low-energy electron diffraction (LEED). In the first chamber, a 100-μm-thick W(001) single crystal was used to allow stress measurements. When depositing Co on one side of this thin crystal it slightly bends due to the stress in the growing film. The bending of the sample is determined by optical deflection of a laser beam which allows us to measure stresses in films down to submonolayer thicknesses.[21] Measurements of the film stress were carried out during deposition. Additionally, the in-plane magnetization was measured using the longitudinal magneto-optic Kerr effect (MOKE) after deposition and the magnetoelastic coupling of the Co films was measured directly by a curvature technique.[3] In the second chamber, besides AES, MOKE, and LEED, additionally a scanning tunneling microscope (STM) is installed to study the surface morphology. In this chamber, a bulk W(001) crystal was used as a substrate. The W(001) samples in both setups were cleaned in the usual way by cycles of glowing in O_2 ($\approx$1700 K, 10^{-7} mbar) and flashing to $\approx$2500 K in the absence of O_2 until no contaminations were detected by AES, and LEED showed sharp (1×1) diffraction patterns. Additionally, STM images of the W(001) crystal revealed clean, flat terraces of sizes larger than 100 nm, separated by single atomic steps. Co (99.99% purity) was deposited by electron beam evaporation. The coverages were calibrated in pseudomorphic monolayers (ML) with STM for STM and LEED experiments and with a quartz microbalance for MOKE and stress measurements, where 1 ML Co corresponds to 1.0×10^{15} atoms/cm^2 or 0.134 nm Co film thickness. Coverages in both experimental setups were cross-related by AES peak intensities, the occurrence of superstructure spots in LEED, and the onset of magnetization determined with MOKE. During growth, the samples could be heated to different temperatures measured with thermocouples attached to the sample holders in close vicinity of the samples. After growth, *in situ* characterization of the film structure, morphology, and magnetism was carried out at room temperature by LEED, STM, and MOKE, respectively.

III. RESULTS AND DISCUSSION

First, we concentrate on the evolution of film stress during growth at room temperature (300 K). Figure 1 displays the stress as a function of film thickness. At 0 ML thickness, deposition was started by opening the shutter of the evaporator and at 18 ML deposition was stopped. Surprisingly, the

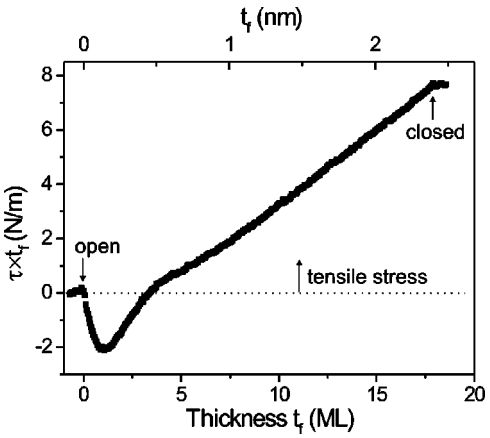

FIG. 1. Integrated film stress $\tau \times t_f$ as a function of Co film thickness t_f measured during film growth at room temperature (300 K). The shutter of the evaporator was opened at 0 ML.

integrated stress initially is compressive with a minimum at ≈ 1 ML followed by a steep increase up to a coverage of ≈ 3 ML where a kink in the stress curve is observed. After the kink, the integrated stress increases with a lower rate. The film stress is given by the slope of the integrated stress curve and corresponds to 7.7 GPa and 3.6 GPa in the region before and after the kink, respectively. At submonolayer coverage, LEED shows sharp (1×1) diffraction patterns [see Fig. 2(a)] indicating pseudomorphic growth. The initial compressive stress is in contrast to the expected tensile stress due to the mismatch of 9.2% calculated from the bulk atomic radii of Co and W in the (1×1) structure. Similar initial compressive stresses have been observed for Fe/W(001), Fe/W(110), and Ni/W(110) (Refs. 22–24) and have been explained by the relaxation of the surface stress of the W surface upon formation of the ferromagnet-tungsten interface,[25,26] i.e., by an electronic effect. The tensile surface stress of the clean W(001) substrate is partially relaxed due to the adsorption of Co, giving rise to an apparent compressive stress. At a coverage of 1 ML the relaxation of the surface stress is completed and a minimum in the stress is observed, indicating that the Co film wets the W crystal. Growth proceeds in a two-dimensional fashion which is also expected from the lower free surface energy of Co in comparison to that of W. STM shows [see Fig. 2(b)] that the film consists of two atomic levels only, the bare W substrate displayed in black and Co islands of monoatomic height in gray. No nucleation of second layer Co islands was found even at coverages close to the completion of the first layer. Upon growth of the second layer a steep rise in the stress can be seen, which corresponds to a tensile stress of 7.7 GPa. This large tensile stress exceeds the elasticity limit of bulk Co by a factor of 3–4; however, the LEED patterns still show a (1×1) structure indicating a fully strained film. The plastic strain relief by formation of dislocations is suppressed. This is a common phenomenon in thin films supported by a substrate.[27] When calculating the stress from the observed strain of 9.1% using Hooke's law with the elasticity constants of Co, one would expect a much higher tensile stress of ≈ 17 GPa. This discrepancy between the observed and the calculated stress can

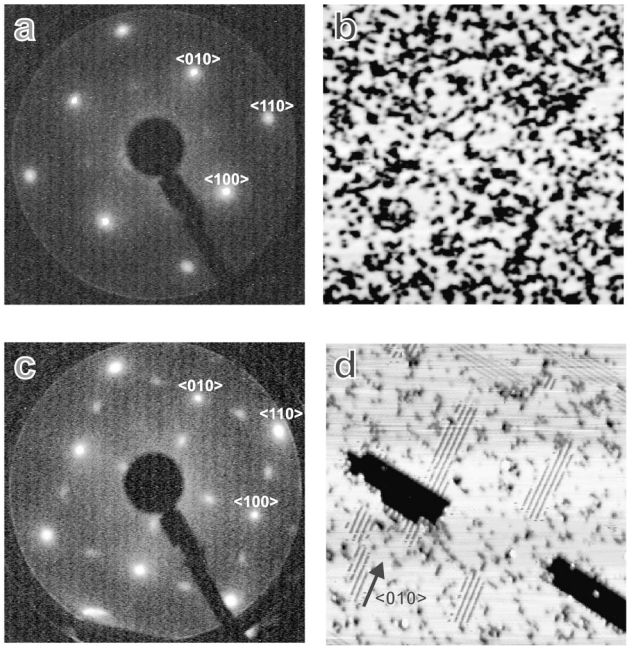

FIG. 2. (a),(c) LEED diffraction pattern at 73 eV and (b),(d) 25×25 nm^2 STM images of the morphology of ≈ 0.8 ML Co on W(001). (a),(b) represent as-grown states (300 K) and (c),(d) are recorded after annealing to ≈ 800 K. Before annealing, (b) shows the bare W substrate (black) and small Co islands of monoatomic height (grey). After annealing, (d) shows large, monoatomic vacancies (black) in the W substrate and small (2×1) reconstructed areas (fine lines) in the Co film.

be understood qualitatively. At these high strains, the linear elastic theory predicts too high stresses, since for large strains, the elastic forces between the Co atoms deviate from Hooke's law due to the anharmonicity of the interaction potential. When the thickness of the film exceeds ≈ 2.7 ML, the stress curve displays a kink and the stress is reduced to 3.6 GPa.

When growth is stopped during the deposition of the first monolayer and the film is annealed to ≈ 800 K, the (1×1) LEED pattern changes into a two-domain (2×1) pattern, as can be seen in Fig. 2(c). This indicates the formation of ordered structures on the surface. AES shows no traces of oxygen or carbon ruling out O- or C-driven reconstructions. To investigate the nature of the ordering, STM measurements have been carried out. Figure 2(d) depicts the surface after annealing. Two types of domains of perpendicularly oriented fine stripes running along $\langle 001 \rangle$ directions can be seen. The distance between neighboring stripes is twice the atomic distance on the W(001) surface in agreement with the (2×1) LEED pattern. The STM scans also show larger vacancy islands of 1 ML depth in the film, which are neither found on the W(001) surface prior to deposition of Co nor after deposition at 300 K [see Fig. 2(b)]. At the bottom of these vacancy islands one finds stripes of the reconstruction, too. This finding helps to clarify whether the striped patches consist of alternating W and Co atoms, i.e., a surface alloy, or of Co atomic lines and vacancy lines or a (2×1) ripple in the Co film, i.e., structures containing no W atoms. In the case

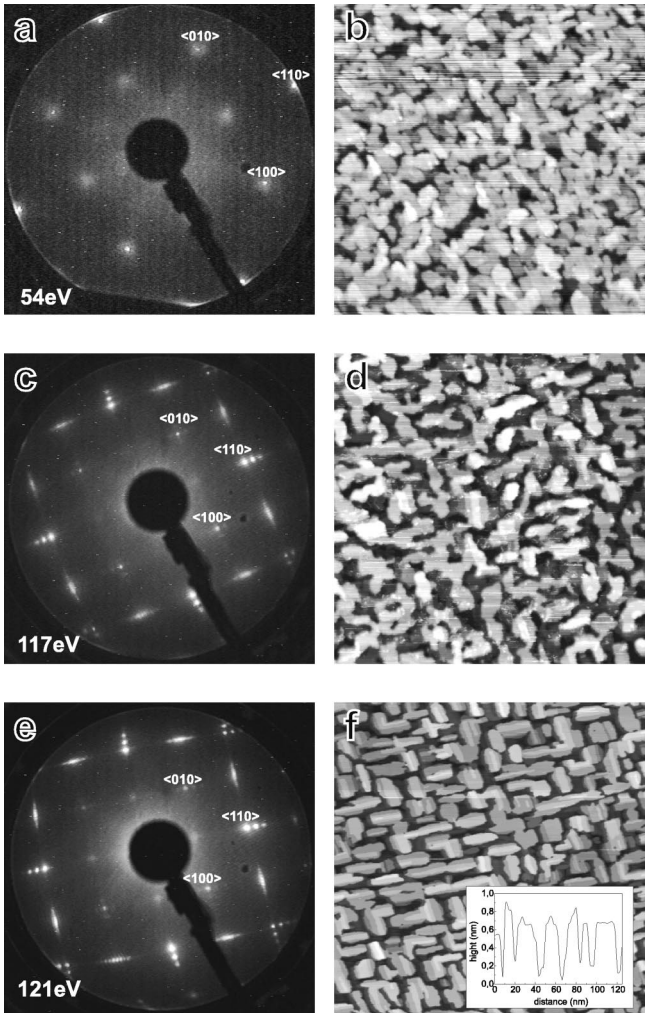

FIG. 3. LEED diffraction pattern (a),(c),(e) and morphology (b),(d),(f) of Co films on W(001) of thicknesses 2.7 ML (a),(b), 5.4 ML (c),(d), and 8.1 ML (e),(f). Deposition was carried out at 300 K (a)–(d) and 330 K (e),(f). LEED patterns were recorded with energies as indicated in the figure. Scales of the STM images are 100 nm×100 nm (b),(d) and 300 nm×300 nm (f). The inset of (f) shows a line scan across the surface.

that the (2×1) stripes are build up entirely of Co atoms, the large vacancies should expose the bare W(001) surface. However, we find stripes also in these vacancies. In the case the stripes consists of an ordered (2×1) CoW alloy, the W surface has to provide some W for the formation of the alloy from its topmost layer. This explains the occurrence of the large vacancy islands on the surface. In addition to this, surface alloying also leads to stripes on the bottom of the vacancy islands. Hence, we can conclude that annealing of submonolayer Co films lead to the formation of an ordered (2×1) CoW alloy. The coverage of (2×1) domains on the surface is, however, more than approximately twice the total area of the vacancies. This indicates that most likely also the preexisting step edges on the W(001) surface act as sources of W atoms for the (2×1) reconstruction. At 300 K, the formation of the alloy is kinetically hindered and observed neither with LEED nor with STM.

During growth at 300 K up to a coverage of $\approx$2.7 ML, the (1×1) LEED pattern is observed, indicating a pseudomorphic and fully strained Co film. As has been deduced from RHEED experiments, this (1×1) structure corresponds to a pseudomorphic bcc Co film.[19,20] Above $\approx$2.7 ML coverage, the LEED pattern changes and additional spots at $\langle\frac{1}{2}\frac{1}{2}0\rangle$ positions appear [see Fig. 3(a)]. Hand in hand with the change of the LEED pattern, the stress measurement shows a kink and the increase of the stress slows down. Wormeester *et al.* related the change in the LEED pattern to a structural change of the film.[19,20] From RHEED experiments they concluded that the structure of the Co films changes from bcc to hcp with the epitaxial relation $(11\bar{2}0)_{\mathrm{Co}}$ parallel to $(001)_{\mathrm{W}}$, when a thickness of 2.4 ML is exceeded.[19,20] Our LEED investigations confirm this phase transformation. The additional $\langle\frac{1}{2}\frac{1}{2}0\rangle$ LEED spots reflect the $c(2\times2)$ superstructure of the four equivalent and nearly quadratic hcp $(11\bar{2}0)$ unit cells, which are rotated by $\pm45°$ with respect to the W(001) unit cell and are larger by a factor of $\sqrt{2}$ (see Fig. 4). The hcp $(11\bar{2}0)$ unit cells show a smaller misfit to the W(001) substrate than the bcc cell. Along the $\langle1\bar{1}00\rangle$ direction of Co, the misfit to the substrate is only 3% while the misfit along $\langle0001\rangle$, i.e., along the *c* axis of Co, is 9.2%. Calculating the expected elastic stress from these misfits with the linear elastic constants of bulk Co and averaging over the four possible orientations of the Co unit cells, however, one expects an even higher stress of $\approx$19 GPa in the film along the W(100) directions. The discrepancy between the expected stress and the observed stress of 3.6 GPa can have different reasons. As can be seen in the STM images of the structure [Fig. 3(b)], the film is rather rough and consists of islands. Our STM observations confirm the findings of Wormeester *et al.*,[19,20] who concluded from the occurrence of RHEED transmission patterns that the film roughens considerably during the transformation from bcc to hcp. The splitting up of the film into small islands might lead to a smaller stress in the film due to a relaxation at the edges of the islands. However, the formation of misfit dislocations in the film is more likely to be responsible for the reduced stress as will be discussed next.

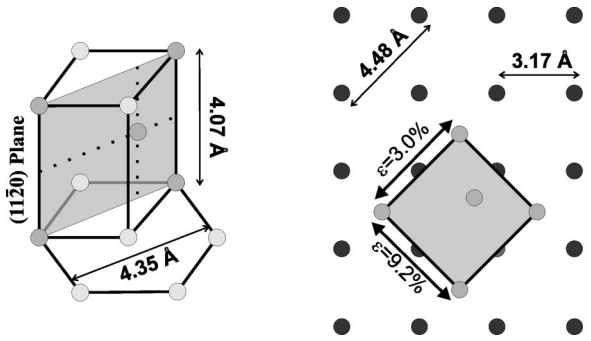

FIG. 4. Schematic drawing of the Co bulk unit cell (left) with the $(11\bar{2}0)$ plane and the structure of the hcp Co film on the W(001) surface (right).

A second mechanism leading to lower stresses in the film is apparent from the LEED patterns of slightly thicker Co films [see Fig. 3(c)]. The LEED spots show a splitting into

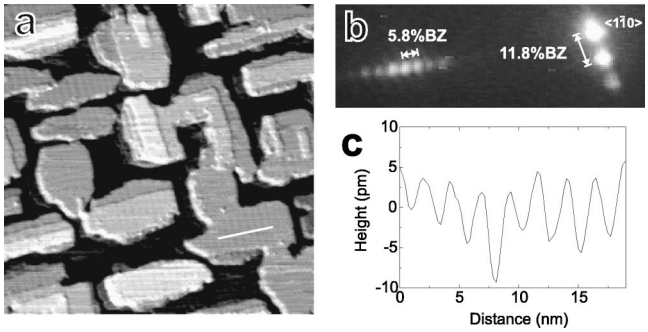

FIG. 5. Medium differentiated STM image of 8.1 ML Co deposited at 330 K (a) showing weak ripples on the top of the islands (100 nm×100 nm). Detail of the LEED diffraction pattern (b) of the same Co film with indications of the splitting of the $\langle 1\bar{1}0\rangle$ spot (right) and the $\langle \frac{1}{2}\frac{\bar{3}}{2}0\rangle$ (left) in percent of the Brillouin zone. Height profile along $\langle 110\rangle$ direction measured with STM on top of an island as indicated by the white line (c).

sets of spots, indicating a superstructure of large lateral dimensions. This splitting of the spots is always visible, as soon as the hcp spots appear. The splitting is, however, rather faintly visible for the thinner films. They become clearer at thicknesses above ≈5 ML. The corresponding STM images [see Fig. 3(d)] reveal that the Co islands have an elongated but irregular shape along the $\langle 110\rangle$ directions of the underlying substrate, most likely reflecting the two possible orientations of the *c* axis of hcp Co on W(001). We carried out measurements with varying deposition temperature and film thickness to optimize the sharpness of the superstructure spots and found the best conditions at slightly elevated growth temperatures of 330 K and thicknesses around 8 ML. There the splitting of the spots is clearly resolved [see Fig. 3(e)]. The spots that correspond to the diffraction conditions of the W(001) show a splitting along the $\langle 110\rangle$ directions of the substrate. The additional spots of half order due to the hcp unit cell also display a broadening with some fine structure along $\langle 110\rangle$ directions. STM images [Fig. 3(f)] show rather regular and rectangular islands elongated along $\langle 110\rangle$ directions with flat tops. The islands have an average height of ≈0.7 nm over a continuous base of the Co film [see line scan in Fig. 3(f)]. When focusing on the flat islands with STM [see Fig. 5(a)], one recognizes a wavy structure along $\langle 110\rangle$ directions. These weak ripples run perpendicular to the long axis of the islands. Note that the STM image of Fig. 5(a) is slightly differentiated to enhance the visibility of the ripples. Figure 5(c) shows a line scan of the height profile across one of the island tops. The ripples have a height of only 5–10 pm and a periodicity of 2.4±0.3 nm. This ripples in real space should be the cause of the splitting of the LEED spots. As displayed in Fig. 5(b), detailed images of the LEED diffraction pattern show a splitting of the $\langle nm0\rangle$ spots with $n,m=1,2,3,\ldots$. The splitting amounts to 11.8%±0.5% of the surface Brillouin zone (BZ) along the $\langle 110\rangle$ directions. This periodicity corresponds to a distance in real space of 2.7±0.1 nm, in good agreement with the STM observations. Hence, both STM and LEED indicate a superstructure of ≈2.7 nm periodicity along $\langle 110\rangle$. The ripples in STM and the superstructure in the LEED patterns are related to the large misfit of 9.2% of the hcp unit cell along its *c* axis with the W(001) substrate. Films of several ML thickness cannot withstand this strain. To release some of the tensile strain of the layer, misfit dislocations form;[27] i.e., some additional atomic planes have to be introduced in the Co film. These dislocations cause a small wavy deformation giving rise to a faint stripe contrast in the STM images.[28,18] The good long-range order of the dislocations induces the splitting of the LEED spots. The distance between the individual dislocations is given by the ripples in the STM data and splitting of the LEED spots. This means that after every 12th atomic plane along the *c* axis of the fully strained Co film, one extra plane is introduced corresponding to a superstructure cell of 2.68 nm along $\langle 110\rangle$. In this structure, the remaining strain along the *c* axis is only 0.9% as compared to the 9.2% in the dislocation-free structure. The agreement between observed STM and LEED structure and the dislocation model is excellent. It excludes that the observed dislocations are along the $\langle 1\bar{1}00\rangle$ direction, the other possible low-index direction of the Co islands, where the misfit is much lower. Additionally, by observation of the ripples of the dislocation in the STM images, one can obtain the local orientation of the *c* axis of the hcp Co islands. The dislocations run perpendicular to the local *c* axis of the film. This dislocation formation is also responsible for the relatively small stresses observed in our stress measurements. The remaining 3% strain along $\langle 1\bar{1}00\rangle$ and 0.9% strain along $\langle 0001\rangle$ of the film correspond to a stress of 5.1 GPa as calculated for a equipopulated coverage of the four possible oriented domains. This is in reasonable agreement with the observed stress of 3.6 GPa. The somewhat smaller stress of the measurements might be due to the large strains exceeding Hooke's law and to the island structure of the film. Hence, the observed kink in the stress curve at 2.7 ML indicated the formation of dislocations. These structural details have been elucidated by a careful LEED and STM study of the growing film.

Interestingly, the hcp spots, i.e., the spots of the order $\langle n/2\ m/2\ 0\rangle$ with $n,m=1,3,\ldots$, show only a splitting of 5.8% of the BZ along $\langle 110\rangle$ directions [see Fig. 5(b)] and hence indicate a superstructure of twice the size. This means that concerning the hcp structure of the Co film, two dislocations are needed for the full periodicity of the superstructure cell. We relate this finding to the details of the stacking in the hcp films and propose a structural model similar to that of the double hcp structure observed in hcp Pd on W(001).[29,20] The hcp stacking sequence *ABA* is interrupted by the additional plane of atoms of the dislocation of stacking *C*. This means that the additional plane locally shows fcc stacking. The stacking fault leads to twinning in the further stacking which proceeds with *AC*. This stacking sequence maximizes the next nearest neighbor distances in the additional plane of atoms and by this possibly lowers the elastic energy of the core of the dislocation. A second dislocation is then needed to come back to the initial stacking sequence *AB*. Figure 6 shows a schematic drawing of the dislocation.

To study the magnetic properties of the Co films, we carried out MOKE measurements as a function of the film

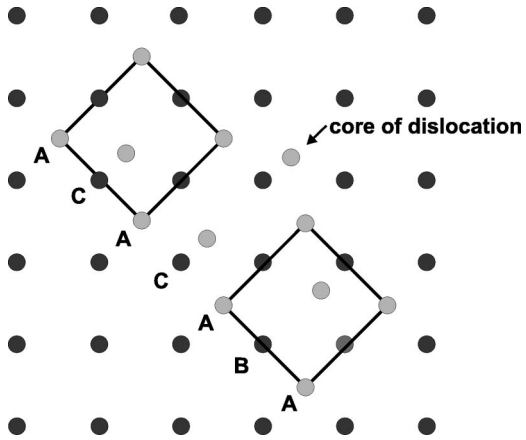

FIG. 6. Top view of a simple model of the stacking around a dislocation of the relaxed Co film.

thickness. All films that revealed a magnetic signal showed an in-plane magnetization. No polar components of the magnetization could be detected. Figure 7 plots the remanent magnetization measured along the ⟨100⟩ direction of the W substrate as a function of the film thickness. The observed longitudinal MOKE signal rises linearly with film thickness as expected. At these low thicknesses, which are below the penetration depth of the photons, the Kerr effect probes the entire film and the observed MOKE signal of the different atomic layers of the film linearly adds up to the total signal. The longitudinal hysteresis loops displayed in the inset of Fig. 7 are of high squareness and the remanence is, within experimental resolution, identical to the saturation. This indicates that the films are easily saturated and complete switching of the film on the scale of the laser spot of the MOKE experiments occurs, most likely not by the nucleation and growth of many domains but by a few domain walls that pass through the film during sweeping of the field. Interest-

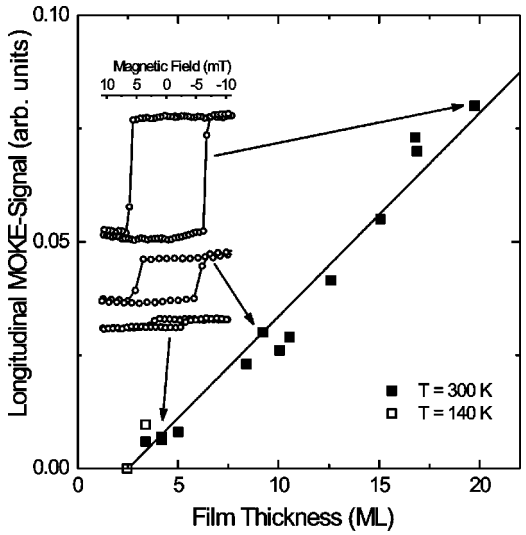

FIG. 7. Longitudinal MOKE signal along the ⟨100⟩ direction of the substrate as a function of Co film thickness grown at 300 K and taken at temperatures as indicated. The inset shows some longitudinal hysteresis loops of film of different thicknesses.

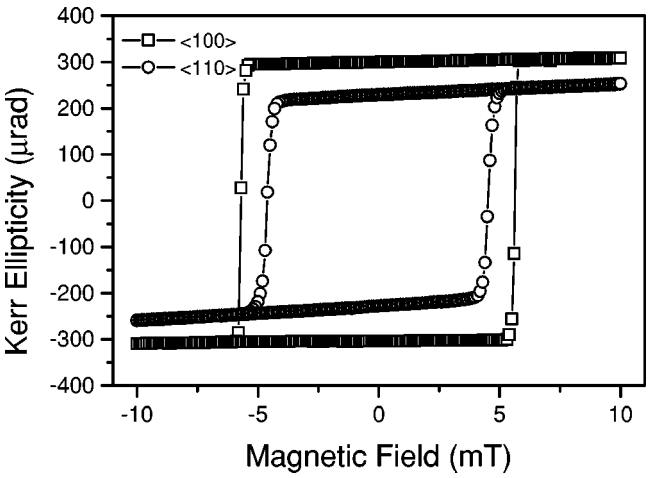

FIG. 8. Longitudinal Kerr magnetization loops of ≈32 ML hcp Co on W(001) along ⟨100⟩ (squares) and ⟨110⟩ (circles) direction of the substrate. The film was grown and measured at 300 K.

ingly, when linearly extrapolating the MOKE signal to low thicknesses, the magnetization vanishes at a coverage of about 2.5 ML. In accordance with this, films as thin as 2.5 ML and thinner did not show any magnetization even upon cooling down to 140 K. This late onset of magnetization, in comparison to Co/Cu(001),[30,11] Co/Cu(111),[15] or Co on other noble metals and Fe on W(001),[31,18] is surprising. The late onset is not due to a late coalescence of the Co film grown at 300 K, as STM indicated an early coalescence at submonolayer coverages [see Fig. 2(b)]. Instead, it seems that a considerable fraction of the film is magnetically dead even at low temperatures. This could be due to a strong electronic hybridization between the Co atoms and the W atoms at the interface suppressing the magnetism at the interface as has been found to be present to some extent in Fe/W(001).[32] Whether the coincidence between the onset of magnetization at ≈2.5 ML and the bcc-hcp phase transition at ≈2.7 ML is just by chance or is related to a possibly nonmagnetic bcc phase of Co on W(001) is unclear and cannot be excluded for our experimental data. Here, first-principles calculations of the magnetic state of bcc Co on W(001) may give a satisfactory answer.

Note that the magnetization curve along ⟨100⟩ displays an almost ideal squareness with full remanence while the loop along ⟨110⟩ shows a reduced remanence of $1/\sqrt{2}$ of the full remanence along ⟨100⟩ (see Fig. 8) and a small positive slope in the two outer branches of the hysteresis loop. This slope can be ascribed to reversible rotation processes at magnetic fields beyond the coercive field. Obviously, the easy direction of magnetization does not lie along the ⟨110⟩ direction as expected from the orientation of the local *c* axis of the Co islands of the film but lies along the ⟨100⟩ direction, i.e., is rotated by 45° with respect to the expected local easy axis of the hcp Co islands. Further, no difference in the magnetic behavior along equivalent ⟨100⟩ directions was found, indicating the absence of a uniaxial contribution to the magnetic anisotropy and showing that the lowest nonvanishing contribution is of fourfold symmetry. To get quantitative data on the fourfold magnetic anisotropy, we used a method that

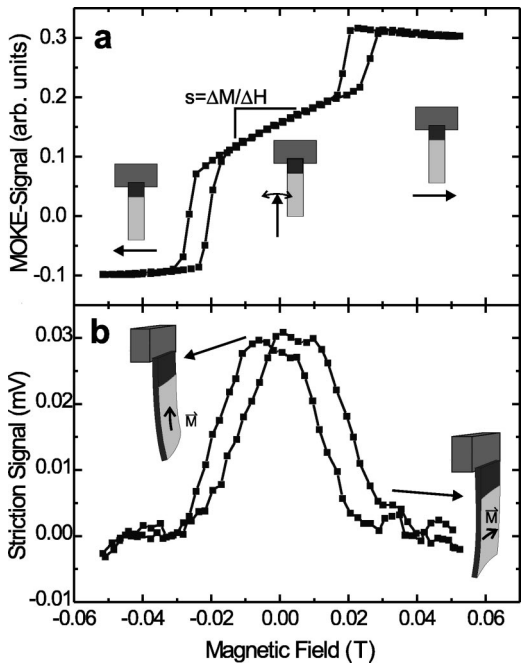

FIG. 9. (a) Horizontal magnetization loop of a ≈5.6-nm-thick hcp Co film along the ⟨100⟩ direction of the substrate with an additional vertical field of 2 mT. (b) Striction signal as a measure of the bending of the sample due to the magnetostriction of the Fe film. The film was grown and measured at 300 K.

was recently introduced.[33,34] By applying an additional constant vertical in-plane field of 2 mT perpendicular to a varying in-plane horizontal field [see Fig. 9(a)], magnetic switching by domain formation is partly suppressed and rotation processes can be observed. From the linear slope s around the center of the hysteresis loop, the fourfold magnetic anisotropy constant can be determined, $K_4=\mu_0 M_s/2s$, where we take in good approximation the saturation magnetization M_s of bulk cobalt. The slope s is given in units of relative longitudinal magnetization as compared to M_s over the applied longitudinal magnetic field. The free energy density F is given by

$$F=\frac{K_4}{4}\sin^2 2\phi, \tag{1}$$

where ϕ is the angle between the magnetization and the ⟨100⟩ direction of the substrate. Using this method for relatively thick films between 4 and 18 nm we found a constant fourfold magnetic anisotropy of $K_4\approx 56$ kJ/m^3 with easy axes along the ⟨100⟩ directions of the substrate. The fact that the anisotropy does not depend on the film thickness suggests that it originates from the interior of the film and is no surface or interface anisotropy; i.e., the anisotropy is a bulk anisotropy. Also, in these quantitative experiments, we found no sign of a uniaxial anisotropy, although the deposited hcp Co is a strongly uniaxial material. The absence of a uniaxial anisotropy can be explained by an equal population of the two possible orientations of the local c axis of the hcp islands. When using an integrating technique like MOKE, the anisotropy is averaged over the area of laser spot and the two uniaxial contributions of the different islands cancel out. Further, the islands are coupled by the magnetic exchange in such a way that the islands do not behave like individual entities but are coupled and the local anisotropy is averaged. This averaging occurs over distances of the width of a magnetic domain wall in Co of the order of ≈16 nm,[35] which is comparable to the island sizes after room-temperature growth. As a result of this averaging, the first-order uniaxial terms of the magnetocrystalline anisotropy of the two-component system proportional to K_1 add up to a constant and do not contribute to the angular dependence of the anisotropy energy, as is obvious from the following expression of the free energy density F:

$$\begin{aligned} F &= \tfrac{1}{2}\,(K_1\sin^2\theta + K_2\sin^4\theta + K_1\cos^2\theta + K_2\cos^4\theta) \\ &= \frac{K_2}{2}(\sin^4\theta + \cos^4\theta) + c = \frac{K_2}{4}(1+\sin^2 2\phi) + c, \end{aligned} \tag{2}$$

where θ is the angle between the magnetization and the ⟨110⟩ direction and K_1 and K_2 are the uniaxial anisotropy constants of first and second-order, respectively, of hcp Co. The second order uniaxial anisotropy terms proportional to K_2, however, do not cancel out and lead to an effective anisotropy of identical angular dependence as the fourfold magnetic anisotropy of Eq. (1); i.e., by the coupled uniaxial islands an effective fourfold anisotropy is created. Taking this model and using the second-order uniaxial anisotropy constant of bulk hcp Co from the literature,[35] $K_2\approx +100$ kJ/m^3, one expects to see a fourfold magnetic anisotropy with easy axes along ⟨100⟩ in agreement with the experimental observation. The observed fourfold anisotropy with easy direction along ⟨100⟩ can hence be understood on the basis of detailed LEED and STM measurements of the structure and morphology of the films. The size of the expected fourfold magnetic anisotropy, however, is by a factor of 2 larger than the observed one. The origin for this discrepancy is unclear. Possibly, the modified hcp structure with the fcc stacking faults in the islands influences the magnetocrystalline anisotropy. Further, the remaining strain in the Co films may also influence the second-order uniaxial magnetic anisotropy via a magnetoelastic coupling constant of higher order in the angular dependence. This will be discussed in more detail in a forthcoming publication.

The particular arrangement of the magnetic fields ensures that the magnetic film is magnetized along the long axis of the W(001) crystal at low fields and along the short axis of the crystal at high fields [see Fig. 9(a)], i.e., for the limits of zero field and high variable magnetic field, the magnetization points to two perpendicular ⟨100⟩ directions. This allows us to determine the magnetostrictive forces in the thin film by observing the bending of the W crystal and from this the magnetoelastic coupling B_4 as a function of film thickness.[36] As depicted in Fig. 9(b), a minute bending of the substrate is detected during the change of the magnetization direction. The radius of curvature of the W substrate for 3 ML Co films is of the order of 40 km. From this small bending, the magnetoelastic stress is calculated as a function of film thickness. The results of the magnetoelastic stress measurements are

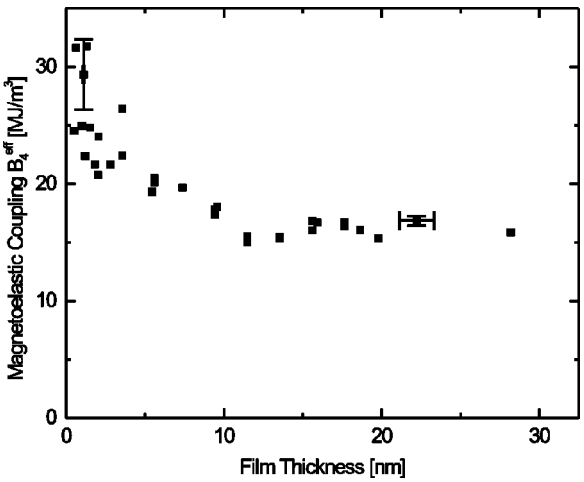

FIG. 10. Effective magnetoelastic coupling $B_e^{\text{eff}}$of Co films on W(001) as a function of film thickness t_f.

plotted in Fig. 10. As can be seen, the magnetoelastic coupling B_4^{eff} of the films is not constant but varies with film thickness and is not identical to the value of $B_4^{bulk} = 37.5$ MJ/m^3 of bulk hcp Co even for relatively thick films.[36] Such deviations of the magnetoelastic coupling of thin films compared to bulk materials are common and have been found for Fe/MgO,[37] Fe/W(001),[22] and Ni/Cu(001).[38] The deviation in these systems has found to be due to a strain-dependent magnetoelastic coupling constant. For large strains, the magnetoelastic contributions to the free energy of the films are no longer proportional to the strain ϵ but a quadratic term in ϵ has to be added.[22,36–38] This becomes obvious when plotting the observed magnetoelastic constant B_4 not as a function of the film thickness, but of the film strain as depicted in Fig. 11. The film strain ϵ has been determined from the observed stress and the elastic constants of Co. The observed magnetoelastic couplings as a linear function of the strain and hence the effective magnetoelstic coupling B_4^{eff} can be expressed as $B_4^{\text{eff}} = B_4 + D_4\epsilon$. The slope D_4 of the linear fit is 1350 ± 120 MJ/m^3 and the axis intercept at $\epsilon = 0$ is 3.4 ± 1.3 MJ/m^3. The slope D_4 is in size

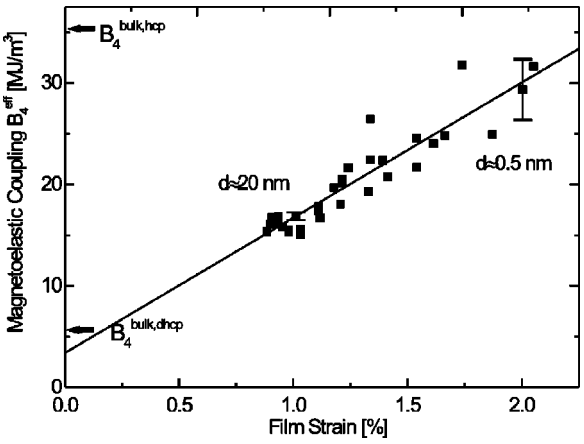

FIG. 11. Effective magnetoelastic coupling of Co films on W(001) as a function of film strain.

comparable to those found for Fe on MgO(001), W(001), and Ni on Cu(001).[37,22,38] The extrapolated intercept is much smaller then the expected magnetoelastic constant B_4 of 37 MJ/m^3 of bulk hcp Co. This discrepancy is most likely due to the different structure of the Co films containing many stacking faults. At the stacking faults, fcc stacking is found and the results of the films including the stacking faults cannot be compared directly to hcp Co. There are studies of the magnetoelastic constant B_4 in bulk Co-rich Fe-Co alloys which display a high density of the same stacking faults.[39,40] The measurements on these alloys indicate that the effective magnetoelastic coupling $B_4^{\text{bulk,dhcp}}$ is strongly reduced to values between 5.6 and 7.7 MJ/m^3 as indicated in Fig. 11. This strong correlation between structure and magnetoelastic coupling is a possible explanation for the low values found in Co films on W(001).

IV. CONCLUSIONS AND SUMMARY

In conclusion, we have studied the relation between stress, strain, and structure and their influence on magnetism of thin Co films of W(001). The interplay between stress, strain, and structure was illuminated by a combination of stress measurements with a bending substrate method and with structural data obtained with LEED and STM. Below ≈ 2.7 ML, the Co film grows pseudomorphically and fully strained as indicated by a simple (1×1) LEED pattern. In contrast to the expected tensile stress, we observed a compressive stress for the first ML which is related to the partial relief of the high surface stress of W(001) upon deposition of Co. In accordance with this effect which is related to the lower free surface energy of Co compared to that of W, the Co film wets the W(001) surface and growth proceeds in a two-dimensional manner, as observed with STM. For higher thickness, tensile stresses are observed in agreement with the atomic radii of Co and W. For the low coverages, the W substrate dictates the structure of the Co film and, hence, in this regime the pseudomorphic structure determines the stress and the strain of the growing film. These bcc Co films up to 2.7 ML are found to be nonmagnetic as checked by MOKE even at low temperatures. However, it is not clear if this is a mere coincidence or related to the bcc structure of the films. At coverages of ≈ 2.7 ML a bcc to hcp phase transition is observed hand in hand with the formation of dislocations in the hcp islands. For these thicker films, the stresses for a pseudomorphic structure would be too large and hence the enormous strain drives the transition to a dislocated hcp structure. The detailed structure of the dislocated films has been analyzed with STM and LEED, and periodic stacking faults induced by the dislocations have been found. The observed remaining tensile stress in the thicker films is in good agreement with the structural model using simple linear elasticity theory. MOKE measurements indicated an in-plane magnetization in the hcp Co films of fourfold magnetic anisotropy with easy directions of magnetization along the $\langle 100 \rangle$ directions of the substrate. This easy direction 45° tilted away from the bulk hcp Co easy axis is explained on the basis of magnetic exchange coupling across individual hcp Co islands resulting in an averaging of the local anisot-

ropy. This averaging cancels out the lowest-order uniaxial anisotropy and only the second-order uniaxial anisotropy is left inducing an effective fourfold behavior. The easy directions of magnetization are correctly explained by this structural model; however, the size of the observed anisotropy is by a factor of 2 higher. This might be a result of the residual strain of the film or the dislocated structure. Further, the magnetoelastic coupling in thin Co films was found to deviate significantly from that of bulk hcp Co, most likely due to the high density of stacking faults in the films. Finally, a new CoW (2×1) surface alloy at low Co coverages has been found.

ACKNOWLEDGMENTS

The authors acknowledge discussions with U. Gradmann and H. Wormeester.

[1] *Ultrathin Magnetic Structures*, edited by J. A. C. Bland and B. Heinrich (Springer-Verlag, Berlin, 1994), Vols. 1 and 2.
[2] M. T. Lin, J. Shen, W. Kuch, H. Jenniches, M. Klaua, C. M. Schneider, and J. Kirschner, Surf. Sci. **410**, 290 (1998).
[3] D. Sander, Rep. Prog. Phys. **62**, 809 (1999).
[4] G. A. Prinz, Phys. Rev. Lett. **54**, 1051 (1985).
[5] L. Gonzalez, R. Miranda, M. Salmeron, J. A. Verges, and F. Yndurain, Phys. Rev. B **24**, 3245 (1981).
[6] A. Clarke, G. Jennings, R. F. Willis, P. J. Rous, and J. B. Pendry, Surf. Sci. **187**, 327 (1987).
[7] C. M. Schneider, P. Bressler, P. Schuster, J. Kirschner, J. J. de Miguel, and R. Miranda, Phys. Rev. Lett. **64**, 1059 (1990).
[8] D. Renard and G. Nihoul, Philos. Mag. B **55**, 75 (1987).
[9] E. Bauer, Appl. Surf. Sci. **11-12**, 479 (1982).
[10] L. Pizzagalli, D. Stoeffler, and F. Gautier, J. Magn. Magn. Mater. **154**, 213 (1996).
[11] P. Krams, F. Lauks, R. L. Stamps, B. Hillebrands, and G. Güntherodt, Phys. Rev. Lett. **69**, 3674 (1992).
[12] A. Berger, U. Linke, and H. P. Oepen, Phys. Rev. Lett. **68**, 839 (1992).
[13] J. Chen and J. Erskine, Phys. Rev. Lett. **68**, 1212 (1992).
[14] U. Gradmann and J. Müller, Phys. Status Solidi **27**, 313 (1968).
[15] F. Huang, M. T. Kief, G. J. Mankey, and R. F. Willis, Phys. Rev. B **49**, 3962 (1994).
[16] W. L. O'Brien and B. P. Tonner, Phys. Rev. B **49**, 15 370 (1994).
[17] D. Sander, A. Enders, and J. Kirschner, J. Magn. Magn. Mater. **200**, 439 (1999).
[18] W. Wulfhekel, F. Zavaliche, F. Porrati, H. P. Oepen, and J. Kirschner, Europhys. Lett. **49**, 651 (2000).
[19] H. Wormeester, E. Hüger, and E. Bauer, Phys. Rev. Lett. **77**, 1540 (1996).
[20] H. Wormeester, E. Hüger, and E. Bauer, Phys. Rev. B **54**, 17 108 (1996).
[21] D. Sander, A. Enders, and J. Kirschner, Rev. Sci. Instrum. **66**, 4734 (1995).
[22] A. Enders, D. Sander, and J. Kirschner, J. Appl. Phys. **85**, 5279 (1999).
[23] D. Sander, R. Skomski, C. Schmidthals, A. Enders, and J. Kirschner, Phys. Rev. Lett. **77**, 2566 (1996).
[24] D. Sander, C. Schmidthals, A. Enders, and J. Kirschner, Phys. Rev. B **57**, 1406 (1998).
[25] D. Sander, A. Enders, and J. Kirschner, Europhys. Lett. **45**, 208 (1999).
[26] D. Sander, C. Schmidthals, A. Enders, and J. Kirschner, Phys. Rev. B **57**, 1406 (1998).
[27] See, e.g., I. Markov, *Crystal Growth for Beginners* (World Scientific, London, 1995).
[28] J. V. Barth, H. Brune, G. Ertl, and R. J. Behm, Phys. Rev. B **42**, 9307 (1990).
[29] S. Prigge, H. Roux, and E. Bauer, Surf. Sci. **107**, 101 (1981).
[30] C. M. Schneider, P. Bressler, P. Schuster, and J. Kirschner, Phys. Rev. Lett. **64**, 1059 (1990).
[31] H. J. Elmers and J. Hauschild, Surf. Sci. **320**, 134 (1994).
[32] R. Wu and A. J. Freeman, Phys. Rev. B **45**, 7532 (1992).
[33] W. Weber, R. Allenspach, and A. Bischof, Appl. Phys. Lett. **70**, 520 (1997).
[34] Y. Millev, H. P. Oepen, and J. Kirschner, Phys. Rev. B **57**, 5848 (1998).
[35] E. Kneller, *Ferromagnetismus* (Springer, Berlin, 1962).
[36] Th. Gutjahr-Löser, D. Sander, and J. Kirschner, J. Magn. Magn. Mater. **220**, L1 (2000).
[37] R. Koch, M. Weber, and K. Rieder, J. Magn. Magn. Mater. **159**, L11 (1996).
[38] T. Gutjahr-Löser, D. Sander, and J. Kirschner, J. Appl. Phys. **87**, 5920 (2000).
[39] T. Wakiyama, H. A. Brooks, E. M. Gyorgy, K. J. Bachmann, and D. Brasen, J. Appl. Phys. **49**, 4158 (1978).
[40] S. Ishio and M. Takahashi, J. Magn. Magn. Mater. **46**, 142 (1984).